Diamond & Related Materials 119 (2021) 108565

Contents lists available at ScienceDirect

Diamond & Related Materials

journal homepage: www.elsevier.com/locate/diamond

Simultaneous reduction and functionalization of graphene oxide sheets with tannic acid for a strong composite material with multi-modally interactive interfaces

Yoo-Bin Kwon [a], Su-Hyeon Go [b], Changsoon Choi [c], Tae Hoon Seo [d], Beomjoo Yang [e,*], Min Wook Lee [b,*], Young-Kwan Kim [a,*]

[a] Department of Chemistry, Dongguk University-Seoul Campus, 30 Pildong-ro, Jung-gu, Seoul 04620, South Korea
[b] Institute of Advanced Composite Materials, Korea Institute of Science and Technology, San 101, Chudong-ro92, Bongdong-eup, Wanju-gun, Jeollabuk-do 55324, South Korea
[c] Department of Energy & Material Engineering, Dongguk University-Seoul Campus, 30 Pildong-ro, Jung-gu, Seoul 04620, South Korea
[d] Nano-Photonics Convergence Technology Group, Korea Institute of Industrial Technology, 6, Cheomdan-gwagiro 208-gil, Buk-gu, Gwangju 61012, South Korea
[e] School of Civil Engineering, Chungbuk National University, 1 Chungdae-ro, Seowon-gu, Cheongju, Chungbuk 28644, South Korea

ARTICLE INFO

Keywords:
Graphene oxide
Reduction
Eco-friendly
Surface modification
Artificial nacre

ABSTRACT

A multi-modally interactive interface is investigated to develop a strong structural material based on hybridization of graphene oxide (GO) and tannic acid (TA) through cross-linking with coordination and covalent bonds. GO is reduced and functionalized with TA by a simple wet-chemical reaction. The resulting TA-reduced and functionalized GO (TA-RGO) sheets are macroscopically assembled into lamellar structured paper like artificial nacre by vacuum-assisted filtration. The assembled TA-RGO paper is sequentially cross-linked by Fe^{3+} ion and polyethyleneimine (PEI) to form a strong interface through multimodal interactions such as hydrogen bonding, covalent bonding, coordination and π-π interactions. The suspended, assembled and cross-linked TA-RGO sheets are systematically characterized by various analytical tools. By forming the multimodal interactions, the tensile strength, modulus and toughness of GO paper were enhanced from 59.5 ± 4.1 MPa, 7.8 ± 1.4 GPa, and 765 ± 112 kJ/m^3 to 167.7 ± 15.4 MPa, 17.6 ± 0.4 GPa, and 1484 ± 192 kJ/m^3, respectively. Based on the results, we clearly demonstrated TA can be harnessed as a multifunctional agent for reducing, functionalizing and cross-linking RGO sheets to construct a strong structural material by forming multi-modally interactive interfaces.

1. Introduction

Graphene has attracted tremendous research interests from various fields owing to their unique and excellent physicochemical properties such as low density, high electrical and thermal conductivity, surface area, flexibility and mechanical strength. [1,2] Among those properties, the low density, high surface area, flexibility and mechanical strength are highly desired for development of a strong structural material, but the applications of pristine graphene has been restricted by its high cost, low processibility and production yield. [3,4] In this regards, graphene oxide (GO), an oxidized version of graphene with oxygen-containing functional groups, is a promising candidate for fabrication of a strong structural material considering its low cost, high aqueous processibility and chemically tailorable surface resulting from abundant oxygen-containing functional groups. [5,6] Although GO presents inferior intrinsic mechanical properties compared to graphene owing to its defected structures, these heterogeneous structures are composed of intact and defected sp^2 carbon domains can be regarded as merits to develop a structural material because they can provide multi-modal interactions through forming electrostatic, hydrogen bonding, and/or covalent bonding, and π-π interaction which originates from the defected and intact sp^2 carbon structures, respectively. [7–11] Therefore, the ordered assembly of GO into macroscopic fibers, lamellar films, and artificial nacre with cross-linked structures by cations or covalent bonds has been considered as one of the most efficient methods to fabricate a strong and flexible structural material. [10–19]

GO has been extensively explored as a building block to construct strong nanocomposites with functional nanomaterials [20–22] and

* Corresponding authors.
E-mail addresses: byang@cbnu.ac.kr (B. Yang), mwlee0713@kist.re.kr (M.W. Lee), kimyk@dongguk.edu (Y.-K. Kim).

https://doi.org/10.1016/j.diamond.2021.108565
Received 13 July 2021; Received in revised form 5 August 2021; Accepted 10 August 2021
Available online 19 August 2021

brick-and-mortar structure inspired by strong materials in nature such as nacre. [23] For fabrication of strong artificial nacre like structures, the appropriate reduction and surface functionalization of GO are prerequisites because those factors govern the inter-sheet interaction modes. [13,15,24] Tannic acid (TA) is one of the most abundant materials in nature, and it has been extensively explored to reduce and functionalize GO owing to its intrinsic reducing power and high affinity toward GO and reduced GO (RGO) through hydrogen bonding and π-π interaction. [25,26] In addition, TA is an eco-friendly agent with diverse oxygen containing functional groups such as phenol, galloyl and carboxylic acid groups and thus the resulting TA-functionalized RGO (TA-RGO) can be readily processed in aqueous media for biosensor [27], antibacterial treatment [28], organic dye adsorption and oil-water separation [29,30]. TA is also well-known as a natural chelating agent for Fe^{3+} ions and thus readily forms the cross-linked structures by coordinative interaction. It can also be readily cross-linked through formation of covalent bonds with polyethyleneimine (PEI). [31–34] Taken together, TA is a promising candidate as a multifunctional agent for reducing, functionalizing and cross-linking GO sheets with multi-modal interactions.

In this study, we investigated the applicability of TA-functionalized RGO (TA-RGO) as a building block to fabricate a strong structural material like artificial nacre through multi-modal interactions such as hydrogen bonding, coordination and π-π interactions as well as covalent bonding. TA-RGO can be simply synthesized by simultaneous reduction and functionalization of GO in the presence of TA because TA consists of abundant phenol groups which provide both its intrinsic reducing power and affinity to the surface of RGO. [25] The resultant TA-RGO was macroscopically assembled into lamella-structured paper by vacuum assisted filtration and then cross-linked by coordination bonds with Fe^{3+} ions or formation of covalent bonds with PEI, respectively. [31,34] Then, the assembled TA-RGO sheets were also sequentially cross-linked by Fe^{3+} ion and PEI for formation of multi-modal interactions between the interfaces of each TA-RGO sheet. This kind of multi-modally interactive interface is widely observed from the natural strong materials but it has been not explored in the TA-RGO based paper-like structures despite of its high potential. In this regard, the TA treatment and sequential cross-linking of GO sheets can be a promising approach to enhance their mechanical properties. The dispersed, assembled and cross-linked TA-RGO sheets were systematically characterized by using various analytical tools. As a result, we found that the sequentially cross-linked TA-RGO papers exhibited a considerable reinforcement of overall mechanical properties compared to their counterparts such as GO, TA-RGO and individually cross-linked TA-RGO papers, which indicates TA plays important and multiple roles as a reducing, functionalizing and cross-linking agent for the construction of strong structural materials with multi-modal interactions.

2. Material and methods

2.1. Materials

Natural graphite (FP 99.95%) was purchased from Graphit Kropfmühl AG (Hauzenberg, Germany). Potassium permanganate, Sodium nitrate, sodium hydroxide, ethanol, hydrochloric acid, sulfuric acid, ammonium hydroxide (25%) and hydrogen peroxide (30%) were purchased from Daejung Chemicals (Siheung, Korea). Tannic acid was purchased from Duksan reagents (Seoul, Korea). Iron (III) chloride hexanhydrate, ACS, 97.0–102.0% was purchased from Alfa Aesar (Ward Hill, Massachusetts, USA). Polyethylenimine (PEI) with Mw ~ 25,000 was purchased from Aldrich (Seoul, Korea).

2.2. Synthesis of TA-RGO

GO was synthesized by Hummers' method. The detailed protocol was described in our previous report. For the synthesis of TA-RGO, GO was suspended in 25 mL of water at 0.1 mg mL^{-1} and then pH of the GO suspension was adjusted to 10 by adding NH_4OH. 25 mg of tannic acid was added to the GO suspension and heated to 95 °C for 1 h with stirring. After the reaction, the reaction mixture was cooled to room temperature, centrifuged at 15770 rcf, washed with water and re-suspended in water. TA-RGO was obtained by repeating centrifugation and washing processes three time.

2.3. Preparation of GO and TA-RGO papers

GO and TA-RGO were suspended in 50 mL of water at 1 mg mL^{-1} and the resulting suspensions were vacuum-filtered through a cellulose acetate (CA) membrane with pore size 0.45 μm. After completion of filtration, the GO and TA-RGO papers were readily deteched from the CA membrane.

2.4. Fe^{3+} ion cross-linking of TA-RGO paper

Fe^{3+} ion crosslinking was carried out by adding 10 mL of 0.2 mM iron (III) chloride hexanhydrate solution (pH = 8) to the suspension of TA-RGO which is being vacuum-filtered (it should be added before finishing filtration process). After completion of filtration, the obtained paper was dried at 60 °C for 12 h and taken off from a CA membrane.

2.5. PEI cross-linking of TA-RGO paper

The prepared TA-RGO paper was immersed in 10 mL of 0.1 M Trizma-buffer solution (pH = 8) and dried at 60 °C for 12 h.

2.6. Sequential cross-linking of TA-RGO paper with Fe^{3+} ion and PEI

The Fe^{3+} ion and PEI cross-linking processes were sequentially performed with TA-RGO. The resulting paper was washed with water three times and dried at 60 °C for 12 h.

2.7. Characterization

UV–Vis-NIR spectra were recorded with a J670 (Jasco, Japan). Their lateral size was observed by using a NOVA Nano SEM 450 (FEI company, Netherlands). Fourier transform infrared (FT-IR) analysis was performed by using a Nicolet iN10 microscope (Thermo Sciencetific, USA) under a reflective mode. Raman analysis was achieved by using a HORIBA LabRAM (jobin Yvon, France) using an air-cooled He/Ne laser (514 nm) focused through an integral microscope (Olympus BX 41) with a 50× objective lens. X-ray photoelectron spectroscopy (XPS) spectra were obtained by using a Thermo Scientific K-alpha (Thermo VG, USA) using monochromated Al Kα (1486.6 eV). The zetapotential of GO and L-RGO was analyzed by using a Nano ZS (Malvern, UK). Thermogravimetric analysis (TGA) was carried out by using a TGA Q 50 (TA instruments, USA) at a heating rate of 10 °C min^{-1} under nitrogen atmosphere (99.999%). For tensile test, the fabricated papers were cut to approximately 30 mm. For analysis of the mechanical properties of those papers, all papers were characterized by using a universal testing machine (UTM) using a 100 N load cell, 20 mm gauge length and 1 mm min^{-1} loading rate, respectively.

3. Results and discussion

TA-RGO was synthesized by reaction of GO with TA which acts as a multifunctional agent for the reduction, surface functionalization and cross-linking (Fig. 1). The reaction process was monitored by using UV–Vis spectroscopy (Fig. 2a, b, c). UV–Vis spectrum of GO showed the absorption peaks at 228 and 300 nm from the π-π* transition of aromatic C═C bonds and n-π* transition from C═O bonds, respectively. With progress of the reaction, the π-π* transition peak of GO was gradually red-shifted to 280 nm with increase of absorption throughout the visible

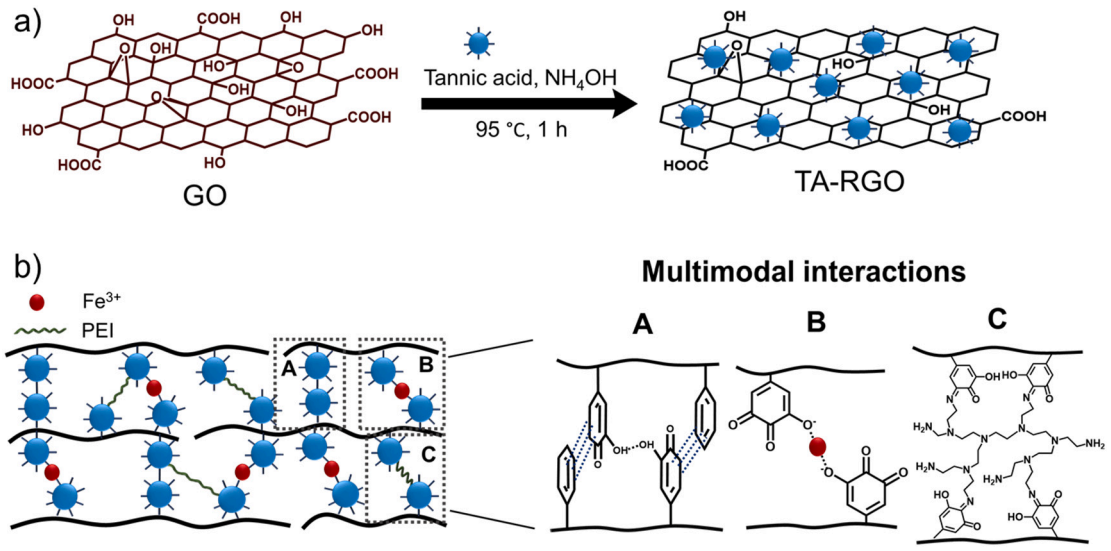

Fig. 1. a) Schematic diagram of synthesis of TA-RGO and b) the multimodal interactions of TA-RGO sheets with Fe^{3+} and PEI.

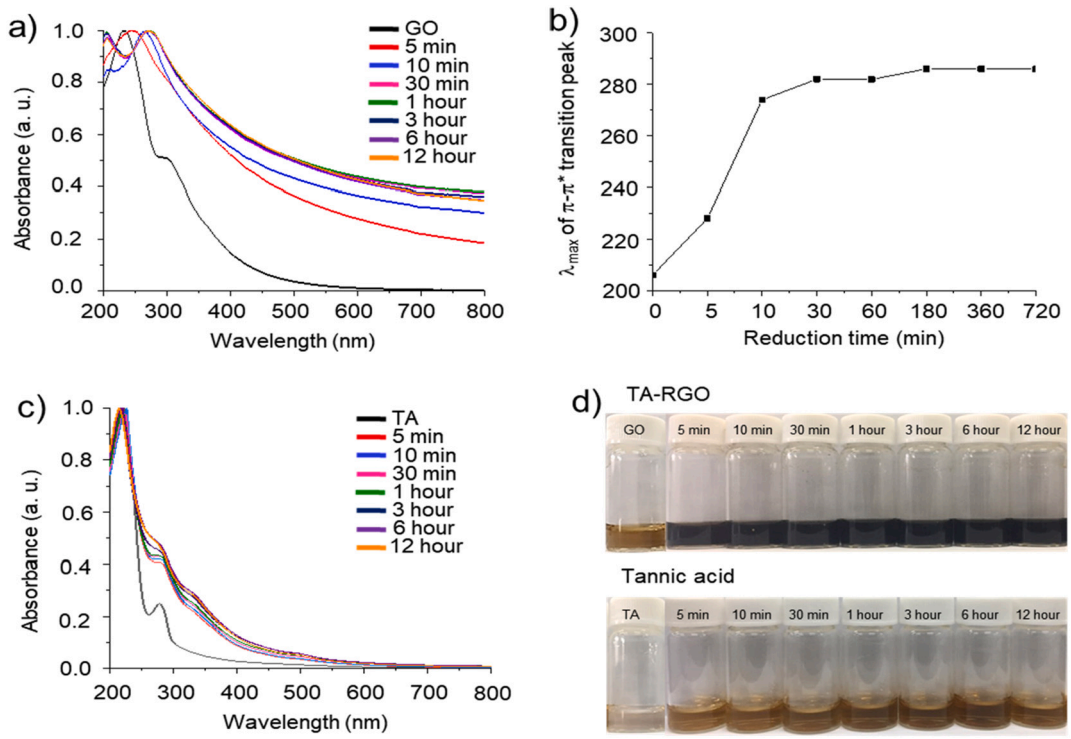

Fig. 2. a) UV–Vis spectra of TA-RGO and b) red-shift of π-π transition peak as a function of reaction time. c) UV–Vis spectra of TA after reaction with GO at different reaction times. d) Photographs of TA-RGO and TA suspension after each reaction time. (For interpretation of the references to color in this figure legend, the reader is referred to the web version of this article.)

region after 1 h and then reached to a plateau (Fig. 2a, b). At the same time, the π-π* transition peak of excess TA in a supernatant of the TA-RGO reaction mixture was blue-shifted from 222 to 216 nm (Fig. 2c). The red- and blue-shift of GO and TA were attributed to the restoration of the conjugated sp^2 carbon domain of GO and the oxidation of its phenolic moieties of TA, respectively. In addition, a new absorbance band at 205 nm appeared in UV–Vis spectra of TA-RGO after 10 min of the reaction and it implied that the oxidized TA derivatives were adsorbed on the surface of RGO (Fig. 2a). [25] Those results indicated the reduction and functionalization of GO with TA are almost completed within 1 h under our reaction condition. The surface charges of GO (−46.0 ± 1.2 mV) became less-negative by the reduction and functionalization with TA; the surface charges of TA-RGO were measured to be (−32.2 ± 2.4 mV). However, it is still highly dispersible in water owing to the surface-adsorbed TA derivatives (Fig. 2d).

The chemical structures of GO, TA, and TA-RGO were characterized with spectroscopic analysis such as FT-IR, Raman, and XPS. FT-IR spectrum of GO showed typical peaks at 3430 cm^{-1} from O—H stretching, 1718 cm^{-1} from C═O stretching, 1625 cm^{-1} from aromatic C═C stretching, 1401 cm^{-1} from O—H deformation, 1382 cm^{-1} from C-OH bending, 1224 cm^{-1} from C-O-C stretching, and 1056 cm^{-1} from C—O stretching (Fig. 3a). [24,35] The characteristic peaks of TA were

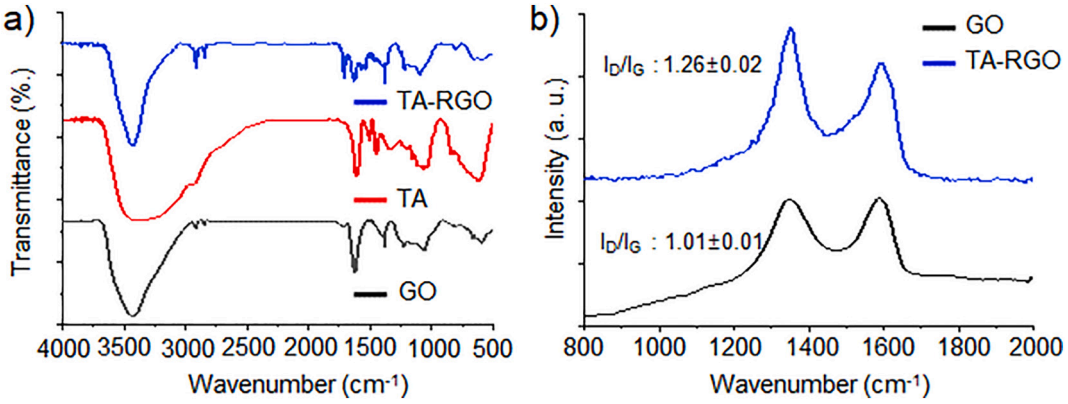

Fig. 3. a) FT-IR spectra of GO, TA, and TA-RGO and b) Raman spectra of GO and TA-RGO respectively.

observed at 3378 cm^{-1} from O—H stretching, 1608 cm^{-1}, 1504 cm^{-1}, and 1450 cm^{-1} from unsaturated aromatic C═C stretching, 1338 $cm^{-1}$from O—H bending, 1033 from C—O stretching (Fig. 3a). [25] In FT-IR spectrum of TA-RGO, even after the reduction process, most of the characteristic peaks from oxygen containing moieties such as O—H stretching, C═O stretching, O—H bending, and C—O stretching were clearly remaining at 3430, 1712, 1382, and 1089 cm^{-1}, respectively. It indicated that the oxidized TA was successfully functionalized on the surface of GO sheets (Fig. 3a). Raman spectrum of GO also presented representative D- and G-peaks at 1347 and 1589 cm^{-1} which are derived from the disordered and intact sp^2 carbon structures, respectively. The relative intensity ratio of D- and G-peaks (I_D/I_G) from GO was determined to be 1.01 ± 0.01 but this value increased to 1.26 ± 0.02 from TA-RGO (Fig. 3b). The increase of I_D/I_G by chemical reduction is frequently observed from the previous studies because it leads to the formation of atomic vacancies during removal of oxygen functional groups and small sized sp^2 carbon domain. [36,37] Therefore, those results clearly indicated that GO was successfully reduced and functionalized with TA, and concurred with the results of UV–Vis analysis.

In C 1s XPS spectra, GO showed characteristic peaks at 284.8, 286.8, 288.3 and 289.2 eV from the C═C, C—O, C═O, O-C═O bonds (Fig. 4a). After the reduction, intensities of C—O, C═O bonds were diminished with increase of C═C bond. Furthermore, O-C═O bonds at 289.2 eV was almost disappeared (From C═C bond: 45.5%, C—O bond: 46.5%, C═O bond: 6.5% and O-C═O bond: 1.5% to C═C bond: 51.5%, C—O bond: 45%, C═O bond: 3% and O-C═O bond: 0.5%) (Fig. 4a–c). All results

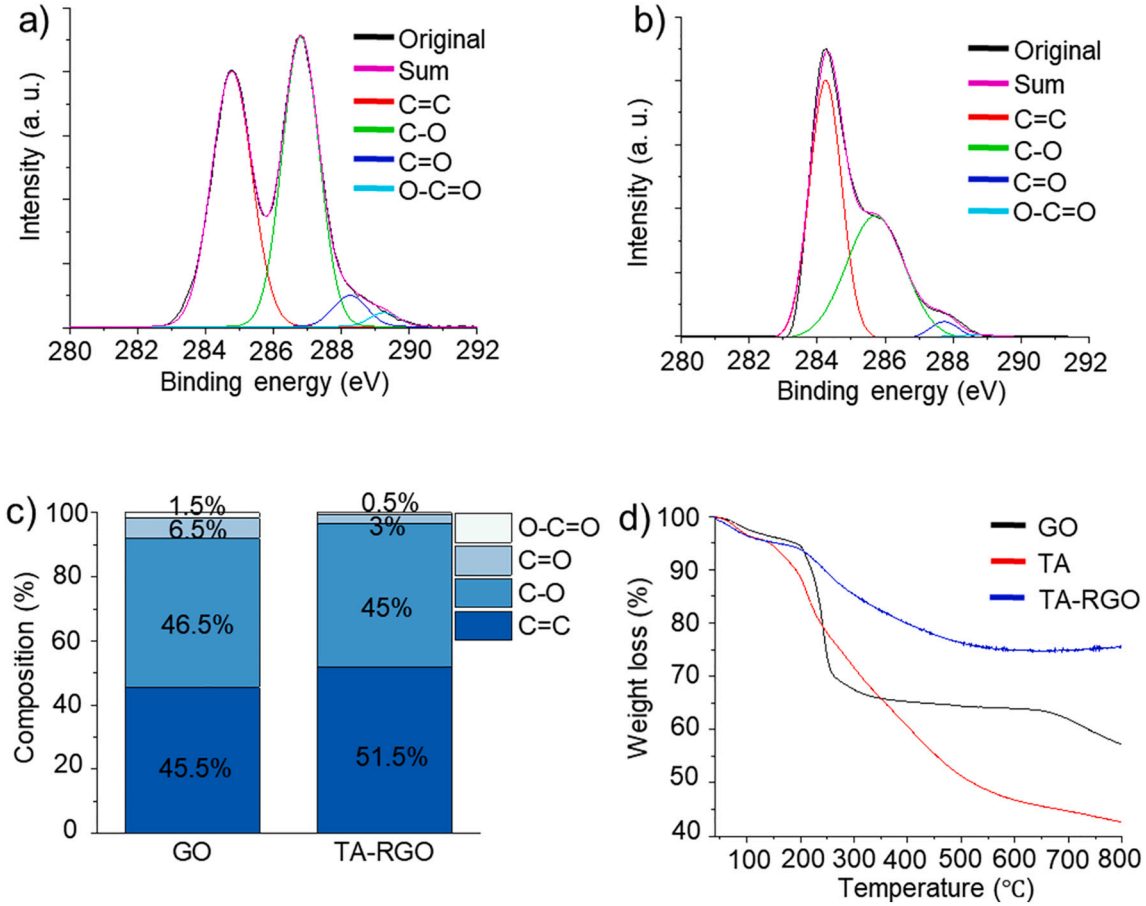

Fig. 4. a) XPS spectra of a) GO, b) TA-RGO. c) Composition of C 1S XPS. d) TGA spectra of GO, TA, TA-RGO.

from the spectroscopic analysis showed the successful functionalization and reduction of GO with TA. The thermal behaviors of GO, TA, TA-RGO were analyzed with TGA. TGA curve of GO showed typical weight loss around 100 °C (2.3%), and 225 °C (12.5%) from evaporation of intercalated water and gasification of oxygen-containing functional groups on GO (Fig. 4d). [37] About 5% weight loss of TA was observed below the 200 °C and it is attributed to gasification of volatiles and water from TA. The major weight loss of TA was observed at around 250 °C (Fig. 4d). [38] After reduction and functionalization, the weight loss of GO around 100 °C and 225 °C increased to 3.6% and decreased to 8%, respectively. The increased weight loss around 100 °C and decreased weight loss around 225 °C were attributed to gasification of volatiles and water from the adsorbed TA molecules, and the diminished oxygen-containing functional groups induced by TA reduction, respectively. The TGA curves of GO, TA, and TA-RGO also elucidate the successful reduction and functionalization of TA to GO sheets (Fig. 4d).

The suspended GO and TA-RGO sheets were assembled into paper-like structures by vacuum assisted filtration and analyzed with XRD to investigate their assembled structures. The representative diffraction peak of GO paper was observed at $2\theta = 11.0°$ corresponding to the (002) plane and d-spacing of 8.03 Å (Fig. 5b). [13] After reduction and functionalization with TA, the diffraction peak from the (002) plane was shifted to $2\theta = 10.5°$ corresponding to the d-spacing of 8.40 Å. The shift of (002) diffraction peak implied the surface of GO sheets was functionalized with TA molecules which enlarged the d-spacing between GO sheets despite of their deoxygenation (Fig. 5b). [25,31,34] To explore the formation of cross-linked structures, TA-RGO paper were treated with Fe^{3+} ions and the d-spacing of TA-RGO papers decreased from 8.40 Å ($2\theta = 10.5°$) to 8.11 Å ($2\theta = 10.9°$) owing to formation of compact Fe^{3+}-TA complexes with coordination interactions. [31] Separately, TA-RGO papers were also treated with PEI and the d-spacing of TA-RGO papers increased from 8.40 Å ($2\theta = 10.5°$) to 9.05 Å ($2\theta = 9.76°$) by intercalation of PEI into TA-RGO sheets followed by formation of covalent bonds between PEI and TA-RGO. [34] Those results indicated TA-RGO sheets possess a potential to form multi-modally interactive interfaces through coordination bonding with Fe^{3+} ions and covalent bonding with PEI. Finally, TA-RGO papers were sequentially treated by Fe^{3+} ions and PEI. The d-spacing of resulting TA-RGO (Fe^{3+}/PEI@TA-RGO) papers was measured to be 8.14 Å ($2\theta = 10.86°$) which is slight larger than that of Fe^{3+} treated TA-RGO (Fe^{3+}@TA-RGO) papers but much smaller than PEI-treated TA-RGO (PEI@TA-RGO) papers (Fig. 5b). These results suggested TA-RGO papers were successfully cross-linked with multi-modal interactions.

For further elucidation of the multi-modal interactions in TA-RGO papers, Fe^{3+}@TA-RGO, PEI@TA-RGO, and Fe^{3+}/PEI@TA-RGO papers were characterized with FT-IR spectroscopy. In FT-IR spectrum of Fe^{3+}@TA-RGO papers, a characteristic peak from Fe—O stretching was observed at 667 cm^{-1} which indicated that the hydroxyl groups in galloyl moieties of TA formed coordination bonds with Fe^{3+} ions (Fig. 5a). [39,40] FT-IR spectrum of PEI@TA-RGO papers presented decrease of a peak at 1712 cm^{-1} from C═O stretching which might originate from the formation of imine structures through Schiff-base reaction between amine groups of PEI and carbonyl groups of TA-RGO (Fig. 5b). [41,42] In the case of Fe^{3+}/PEI@TA-RGO papers, the appearance of Fe—O stretching peak and attenuation C═O stretching peak were simultaneously observed. Especially, although C═O stretching peak of TA-RGO was not affected by cross-linking with Fe^{3+} ions, that of Fe^{3+}/PEI@TA-RGO paper was further diminished in comparison with that of PEI@TA-RGO paper. This change implied that the Fe^{3+} ion cross-linking of TA-RGO paper facilitated formation of imine covalent bonds between PEI and TA-RGO papers. Those results supported the formation of multi-modally interactive interface between TA-RGO sheets consisting of TA-RGO paper.

Finally, influence of interfacial interaction on the mechanical properties of GO and cross-linked TA-RGO papers was explored with tensile experiments by using UTM. As a result of TA reduction and functionalization, the tensile strength and modulus of GO papers slightly increased from 59.5 ± 4.1 to 68.8 ± 3.7 MPa and 7.8 ± 1.4 to 14.3 ± 0.8 GPa (Fig. 6a, b, c), respectively. However, the toughness of GO significantly decreased from 765 ± 112 to 166 ± 170 kJ/m^3 (Fig. 6a, d). The enhanced modulus and decreased toughness are typically observed from the cross-linked GO papers and thus those changes of mechanical properties implied the interaction between GO sheets were strengthened by the surface-adsorbed TA moieties through formation of hydrogen bonding. [43] The cross-linking effect of TA-RGO papers was also revealed with Fe^{3+}@TA-RGO and PEI@TA-RGO papers. The cross-linking of TA-RGO paper with Fe^{3+} ions increased the tensile strength and toughness to 82.8 ± 9.9 MPa and 949 ± 193 kJ/m^3, respectively, but its modulus considerably decreased to 4.3 ± 0.7 GPa. On the other hand, PEI cross-linking of TA-RGO paper enhanced its tensile strength to 100.7 ± 14.2 MPa and toughness to 415 ± 91 kJ/m^3 without decrease of tensile modulus (Fig. 6). Those results showed that the two cross-linking strategies possess the distinct features to design and construct a robust structural material. For instance, Fe^{3+} ion cross-linking drastically increased the toughness with an expense of tensile modulus and, by contrast, PEI cross-linking greatly enhanced the tensile strength accompanied with a moderate increase of toughness and sustained tensile modulus. Therefore, we can expect the synergistic effect of sequential cross-linking treatment with Fe^{3+} ions and PEI on the mechanical properties of TA-RGO papers. As expected, the tensile strength, modulus and toughness of Fe^{3+}/PEI@TA-RGO paper, a model of multi-modally interactive interfaces, reached to 167.7 ± 15.4 MPa, 17.6 ± 0.4

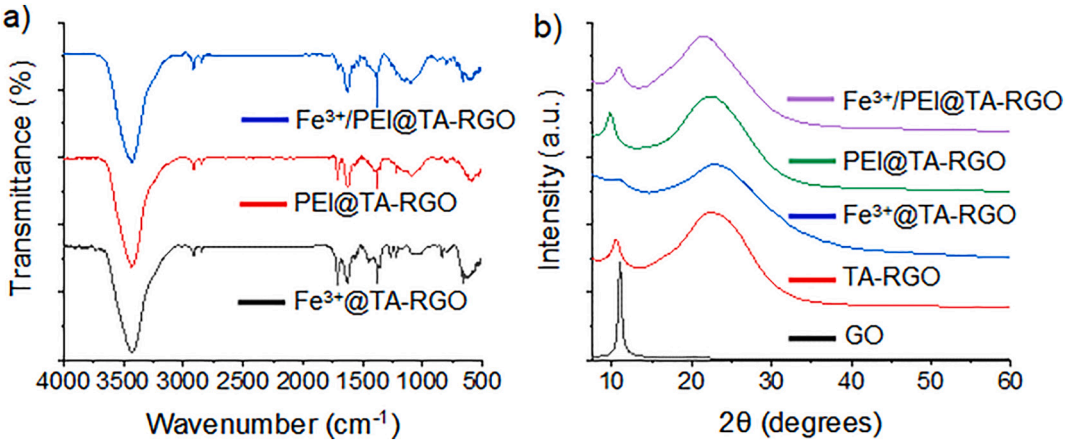

Fig. 5. a) FT-IR spectra of Fe^{3+}@TA-RGO, PEI@TA-RGO, Fe^{3+}/PEI@TA-RGO. b) XRD spectra of GO, TA-RGO, Fe^{3+}@TA-RGO, PEI @TA-RGO, and Fe^{3+}/PEI@TA-RGO paper.

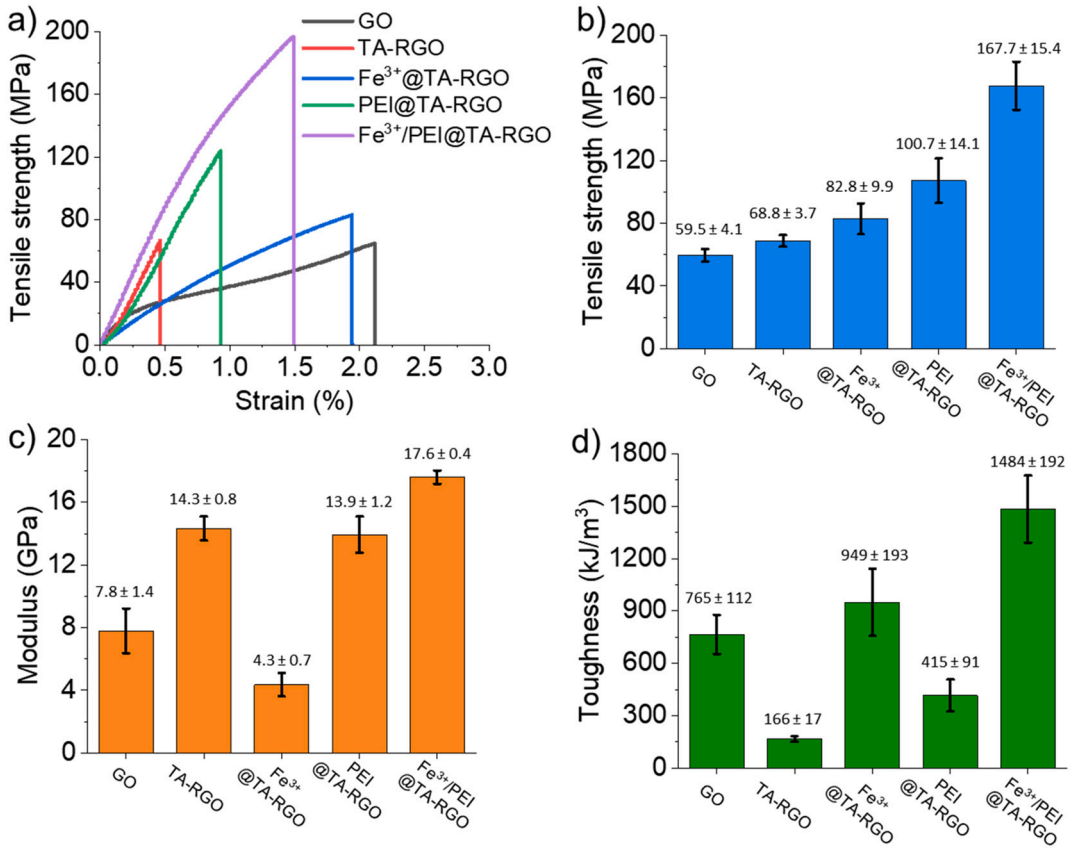

Fig. 6. a) Stress-strain curves, b) tensile strength, c) modulus, and d) toughness of GO, TA-RGO, Fe^{3+}@TA-RGO, PEI@TA-RGO, and Fe^{3+}/PEI@TA-RGO papers, respectively.

GPa and 1484 ± 192 kJ/m^3, respectively (Fig. 6). This overall enhancement of mechanical properties indicated the sequential cross-liking of TA-RGO paper successfully resulted in formation of a multi-modally interactive. As a control, the sequential cross-linking strategy with Fe^{3+} ion and PEI was also applied to GO paper but there was not the overall reinforcement effect. This difference indicated TA reduction and functionalization is essential for the formation of multi-modally interactive interfaces through its galloyl and carbonyl groups for coordination and covalent bonding with Fe^{3+} ion and PEI, respectively (Fig. S1). Taken together, it was clearly demonstrated that the multi-modal interactions such as π-π interactions, hydrogen bonding, coordination and covalent bonding can greatly improve mechanical properties of the hierarchically-structured nanocomposites.

4. Conclusion

In conclusion, we demonstrated TA can be harnessed as a multi-functional agent for the reduction, functionalization, and cross-linking of GO sheets with a multi-modal interaction. TA-RGO sheets were macroscopically assembled into a lamella-structured film, which mimics an artificial nacre, by vacuum-assisted filtration and sequentially cross-linked with Fe^{3+} ions and PEI for formation of coordination and covalent bonding network, respectively. The assembled TA-RGO papers and their counterparts with individual and dual cross-linked structures were systematically characterized to reveal the effect of multi-modal interaction on their structural and mechanical properties. As a result, the sequentially cross-linked Fe^{3+}/PEI@TA-RGO papers showed the considerable enhancement of overall mechanical properties such as the tensile strength, modulus and toughness (167.7 ± 15.4 MPa, 17.6 ± 0.4 GPa and 1484 ± 192 kJ/m^3) which are 2.45, 1.23 and 8.9 folds compared to TA-RGO papers, respectively. Especially, those mechanical properties are also higher than TA-RGO papers cross-linked by individual treatment of Fe^{3+} ions (tensile strength, modulus and toughness are 82.8 ± 9.9 MPa, 4.3 ± 0.7 GPa and 949 ± 193 kJ/m^3) and PEI (tensile strength, modulus and toughness are 100.7 ± 14.1 MPa, 13.9 ± 1.2 GPa and 415 ± 91 kJ/m^3). There was a synergistic effect on the mechanical properties of TA-RGO papers by sequential cross-linking treatments resulting in their overall reinforcement through the formation of multi-modally interactive interfaces. Taken together, it was clearly revealed that crosslinking with both Fe^{3+} and PEI greatly improved the mechanical properties of TA-RGO papers and we believe that the present strategy will be an effective and facile approach to fabricate the mechanically robust graphene-based artificial nacre structure.

Supplementary data to this article can be found online at https://doi.org/10.1016/j.diamond.2021.108565.

CRediT authorship contribution statement

Yoo-Bin Kwon: Methodology, Investigation, Writing – Original Draft. Su-Hyeon Go: Methodology, Data curation. Changsoon Choi: Conceptualization, Validation. Tae Hoon Seo: Data curation, Resources. Beomjoo Yang: Conceptualization, Data curation, Resources. Min Wook Lee: Conceptualization, Data curation, Resources. Young-Kwan Kim: Conceptualization, Supervision, Data curation, Resources, Funding acquisition, Writing – Original Draft

Declaration of competing interest

The authors declare that they have no known competing financial interests or personal relationships that could have appeared to influence the work reported in this paper.

Acknowledgments

This work was supported by the Dongguk University Research Fund of 2019. This research was also supported through the Korea Institute of Industrial Technology (KITECH).

References

[1] K. Geim, Novoselov A., The rise of graphene, Nat. Mater. 6 (2007) 1–265, https://doi.org/10.1007/978-3-319-70329-9.
[2] M.J. Allen, V.C. Tung, R.B. Kaner, Honeycomb carbon: a review of graphene, Chem. Rev. 110 (2010) 132–145, https://doi.org/10.1021/cr900070d.
[3] Y. Zhu, S. Murali, W. Cai, X. Li, J.W. Suk, J.R. Potts, R.S. Ruoff, Graphene and graphene oxide: synthesis, properties, and applications, Adv. Mater. 22 (2010) 3906–3924, https://doi.org/10.1002/adma.201001068.
[4] V.B. Mohan, D.Hui K. tak Lau D. Bhattacharyya, Graphene-based materials and their composites: a review on production, applications and product limitations, Compos. Part B Eng. 142 (2018) 200–220, https://doi.org/10.1016/j.compositesb.2018.01.013.
[5] D.R. Dreyer, S. Park, C.W. Bielawski, R.S. Ruoff, The chemistry of graphene oxide, Chem. Soc. Rev. 39 (2010) 228–240, https://doi.org/10.1039/b917103g.
[6] L. Qiu, D. Li, H.M. Cheng, Structural control of graphene-based materials for unprecedented performance, ACS Nano 12 (2018) 5085–5092, https://doi.org/10.1021/acsnano.8b03792.
[7] D.A. Dikin, S. Stankovich, E.J. Zimney, R.D. Piner, G.H.B. Dommett, G. Evmenenko, S.T. Nguyen, R.S. Ruoff, Preparation and characterization of graphene oxide paper, Nature 448 (2007) 457–460, https://doi.org/10.1038/nature06016.
[8] S. Stankovich, D.A. Dikin, G.H.B. Dommett, K.M. Kohlhaas, E.J. Zimney, E. A. Stach, R.D. Piner, S.B.T. Nguyen, R.S. Ruoff, Graphene-based composite materials, Nature 442 (2006) 282–286, https://doi.org/10.1038/nature04969.
[9] N.V. Medhekar, A. Ramasubramaniam, R.S. Ruoff, V.B. Shenoy, Hydrogen bond networks in graphene oxide composite paper: structure and mechanical properties, ACS Nano 4 (2010) 2300–2306, https://doi.org/10.1021/nn901934u.
[10] O.C. Compton, S.W. Cranford, K.W. Putz, Z. An, L.C. Brinson, M.J. Buehler, S. T. Nguyen, Tuning the mechanical properties of graphene oxide paper and its associated polymer nanocomposites by controlling cooperative intersheet hydrogen bonding, ACS Nano 6 (2012) 2008–2019, https://doi.org/10.1021/nn202928w.
[11] X. Sun, C. Huang, L. Wang, L. Liang, Y. Cheng, W. Fei, Y. Li, Recent progress in graphene/polymer nanocomposites, Adv. Mater. 2001105 (2020) 1–28, https://doi.org/10.1002/adma.202001105.
[12] S. Park, K.S. Lee, G. Bozoklu, W. Cai, S.B.T. Nguyen, R.S. Ruoff, Graphene oxide papers modified by divalent ions - enhancing mechanical properties via chemical cross-linking, ACS Nano 2 (2008) 572–578, https://doi.org/10.1021/nn700349a.
[13] O.C. Compton, D.A. Dikin, K.W. Putz, L.C. Brinson, S.T. Nguyen, Electrically conductive "alkylated" graphene paper via chemical reduction of amine-functionalized graphene oxide paper, Adv. Mater. 22 (2010) 892–896, https://doi.org/10.1002/adma.200902069.
[14] C. Wei, L. Mingzhu, L. Jiyang, W. Ben, Z. Chuck, J. Lei, C. Qunfeng, †Key, strong integrated strength and toughness artificial nacre based on dopamine cross-linked graphene oxide, ACS Nano 8 (2014) 9511–9517.
[15] Z. An, O.C. Compton, K.W. Putz, L.C. Brinson, S.T. Nguyen, Bio-inspired borate cross-linking in ultra-stiff graphene oxide thin films, Adv. Mater. 23 (2011) 3842–3846, https://doi.org/10.1002/adma.201101544.
[16] X. Zhang, X. Fan, C. Yan, H. Li, Y. Zhu, X. Li, L. Yu, Interfacial microstructure and properties of carbon fiber composites modified with graphene oxide, ACS Appl. Mater. Interfaces 4 (2012) 1543–1552, https://doi.org/10.1021/am201757v.
[17] M. Hu, B. Mi, Layer-by-layer assembly of graphene oxide membranes via electrostatic interaction, J. Memb. Sci. 469 (2014) 80–87, https://doi.org/10.1016/j.memsci.2014.06.036.
[18] R.K. Joshi, S. Alwarappan, M. Yoshimura, V. Sahajwalla, Y. Nishina, Graphene oxide: the new membrane material, Appl. Mater. Today 1 (2015) 1–12, https://doi.org/10.1016/j.apmt.2015.06.002.
[19] R. Cruz-Silva, M. Endo, M. Terrones, Graphene oxide films, fibers, and membranes, Nanotechnol. Rev. 5 (2016) 377–391, https://doi.org/10.1515/ntrev-2015-0041.
[20] Q. Wang, Z. Yu, Y. Liu, X. Zhu, R. Long, X. Li, Electrostatic self-assembly method to prepare intercalated graphene oxide composite membrane to improve hydrophilicity and flux, Diam. Relat. Mater. 117 (2021), 108492, https://doi.org/10.1016/j.diamond.2021.108492.
[21] X. Zhao, X. Chen, X. Yu, X. Ding, X.L. Yu, X.P. Chen, Fast response humidity sensor based on graphene oxide films supported by TiO2 nanorods, Diam. Relat. Mater. 109 (2020), 108031, https://doi.org/10.1016/j.diamond.2020.108031.
[22] Z. Jin, Z.Luo S. E D. Ning, Investigations on the thermal conduction behaviors of reduced graphene oxide/aramid nanofibers composites, Diam. Relat. Mater. 116 (2021), 108422, https://doi.org/10.1016/j.diamond.2021.108422.
[23] Q. Cheng, M. Wu, M. Li, L. Jiang, Z. Tang, Ultratough artificial nacre based on conjugated cross-linked graphene oxide, Angew. Chem. Int. Ed. 52 (2013) 3750–3755, https://doi.org/10.1002/anie.201210166.
[24] Y.L. Hong, S. Ryu, H.S. Jeong, Y.K. Kim, Surface functionalization effect of graphene oxide on its liquid crystalline and assembly behaviors, Appl. Surf. Sci. 480 (2019) 514–522, https://doi.org/10.1016/j.apsusc.2019.03.023.
[25] Y. Lei, Z. Tang, R. Liao, B. Guo, Hydrolysable tannin as environmentally friendly reducer and stabilizer for graphene oxide, Green Chem. 13 (2011) 1655–1658, https://doi.org/10.1039/c1gc15081b.
[26] B. Akkaya, B. Çakiroglu, M. Özacar, Tannic acid-reduced graphene oxide deposited with pt nanoparticles for switchable bioelectronics and biosensors based on direct electrochemistry, ACS Sustain. Chem. Eng. 6 (2018) 3805–3814, https://doi.org/10.1021/acssuschemeng.7b04164.
[27] W. Lu, X. Qin, A.M. Asiri, A.O. Al-Youbi, X. Sun, Facile synthesis of novel Ni(ii)-based metal-organic coordination polymer nanoparticle/reduced graphene oxide nanocomposites and their application for highly sensitive and selective nonenzymatic glucose sensing, Analyst 138 (2013) 429–433, https://doi.org/10.1039/c2an36194a.
[28] J. Luo, J. Lai, N. Zhang, Y. Liu, R. Liu, X. Liu, Tannic acid induced self-assembly of three-dimensional graphene with good adsorption and antibacterial properties, ACS Sustain. Chem. Eng. 4 (2016) 1404–1413, https://doi.org/10.1021/acssuschemeng.5b01407.
[29] C.Y. Tang, P. Yu, L.S. Tang, Q.Y. Wang, R.Y. Bao, Z.Y. Liu, M.B. Yang, W. Yang, Tannic acid functionalized graphene hydrogel for organic dye adsorption, Ecotoxicol. Environ. Saf. 165 (2018) 299–306, https://doi.org/10.1016/j.ecoenv.2018.09.009.
[30] A.V. Singhal, R. George, A.K. Sharma, D. Malwal, I. Lahiri, Development of superhydrophillic tannic acid-crosslinked graphene oxide membranes for efficient treatment of oil contaminated water with enhanced stability, Heliyon 6 (2020), e05127, https://doi.org/10.1016/j.heliyon.2020.e05127.
[31] R.Y. Liu, A.W. Xu, Byssal threads inspired ionic cross-linked narce-like graphene oxide paper with superior mechanical strength, RSC Adv. 4 (2014) 40390–40395, https://doi.org/10.1039/c4ra08319a.
[32] V. Ball, High loading capacity of Fe3 cations in LBL films made from poly (ethyleneimine) and tannic acid: an alternative to coordination driven multistep assembly using polyphenols and Fe3, Colloids Interface Sci. Commun. 3 (2014) 1–4, https://doi.org/10.1016/j.colcom.2014.12.002.
[33] Y.M. Li, X. Miao, Z.G. Wei, J. Cui, S.Y. Li, R.M. Han, Y. Zhang, W. Wei, Iron-tannic acid nanocomplexes: facile synthesis and application for removal of methylene blue from aqueous solution, Dig. J. Nanomater. Biostruct. 11 (2016) 1045–1061.
[34] M.Y. Lim, Y.S. Choi, J. Kim, K. Kim, H. Shin, J.J. Kim, D.M. Shin, J.C. Lee, Cross-linked graphene oxide membrane having high ion selectivity and antibacterial activity prepared using tannic acid-functionalized graphene oxide and polyethyleneimine, J. Memb. Sci. 521 (2017) 1–9, https://doi.org/10.1016/j.memsci.2016.08.067.
[35] Z. Çiplak, N. Yildiz, A. Calimli, Investigation of graphene/Ag nanocomposites synthesis parameters for two different synthesis methods, in: Fullerenes Nanotub. Carbon Nanostructures 23, 2015, pp. 361–370, https://doi.org/10.1080/1536383X.2014.894025.
[36] A.C. Ferrari, D.M. Basko, Raman spectroscopy as a versatile tool for studying the properties of graphene, Nat. Nanotechnol. 8 (2013) 235–246, https://doi.org/10.1038/nnano.2013.46.
[37] Y.K. Kim, M.H. Kim, D.H. Min, Biocompatible reduced graphene oxide prepared by using dextran as a multifunctional reducing agent, Chem. Commun. 47 (2011) 3195–3197, https://doi.org/10.1039/c0cc05005a.
[38] Z. Xia, A. Singh, W. Kiratitanavit, R. Mosurkal, J. Kumar, R. Nagarajan, Unraveling the mechanism of thermal and thermo-oxidative degradation of tannic acid, Thermochim. Acta 605 (2015) 77–85, https://doi.org/10.1016/j.tca.2015.02.016.
[39] E.S. Guang Choo, X. Tang, Y. Sheng, B. Shuter, J. Xue, Controlled loading of superparamagnetic nanoparticles in fluorescent nanogels as effective T2-weighted MRI contrast agents, J. Mater. Chem. 21 (2011) 2310–2319, https://doi.org/10.1039/c0jm03232h.
[40] T. Togashi, T. Naka, S. Asahina, K. Sato, S. Takami, T. Adschiri, Surfactant-assisted one-pot synthesis of superparamagnetic magnetite nanoparticle clusters with tunable cluster size and magnetic field sensitivity, Dalt. Trans. 40 (2011) 1073–1078, https://doi.org/10.1039/c0dt01280g.
[41] F. Soyekwo, Q. Zhang, R. Gao, Y. Qu, R. Lv, M. Chen, A. Zhu, Q. Liu, Metal in situ surface functionalization of polymer-grafted-carbon nanotube composite membranes for fast efficient nanofiltration, J. Mater. Chem. A 5 (2017) 583–592, https://doi.org/10.1039/c6ta07567c.
[42] Q. Li, Z. Liao, X. Fang, D. Wang, J. Xie, X. Sun, L. Wang, J. Li, Tannic acid-polyethyleneimine crosslinked loose nanofiltration membrane for dye/salt mixture separation, J. Memb. Sci. 584 (2019) 324–332, https://doi.org/10.1016/j.memsci.2019.05.002.
[43] Z. Liu, H. Fan, W. Li, G. Bai, X. Li, N. Zhao, J. Xu, F. Zhou, X. Guo, B. Dai, E. Benassi, X. Jia, Competitive self-assembly driven as a route to control the morphology of poly(tannic acid) assemblies, Nanoscale 11 (2019) 4751–4758, https://doi.org/10.1039/c8nr07236a.